MISARA: Matlab Interface for Seismo-Acoustic aRray Analysis

Minio, V.[1], Zuccarello[2,3], L., De Angelis[2,3], S., Di Grazia, G.[4], Saccorotti, G.[3]

[1]Dipartimento di Scienze Biologiche, Geologiche ed Ambientali - Sezione di Scienze della Terra, Università degli Studi di Catania, Catania, Italy.

[2]School of Environmental Sciences, University of Liverpool, Liverpool, UK.

[3]Istituto Nazionale di Geofisica e Vulcanologia, Sezione di Pisa, Pisa, Italy.

[4]Istituto Nazionale di Geofisica e Vulcanologia, Sezione di Catania-Osservatorio Etneo, Catania, Italy.

Corresponding authors: Luciano Zuccarello (luciano.zuccarello@ingv.it)

ABSTRACT

Volcanic activity produces a broad spectrum of seismic and acoustic signals whose characteristics provide important clues on the underlying magmatic processes. Networks and arrays of seismic and acoustic sensors are the backbone of most modern volcano monitoring programmes. Investigation of the signals gathered by these instruments requires efficient workflows and specialist software. The high sampling rates, typically 50 Hz or greater, at which seismic and acoustic waveforms are recorded by multi-station networks and dense arrays leads to the rapid accumulation of large volumes of data, making the implementation of efficient data analysis workflows for volcano surveillance a challenging task. Here, we present an open-source Matlab Graphical User Interface (GUI), MISARA (Matlab Interface for Seismo-Acoustic aRray Analysis), designed to provide a user-friendly workflow for the analysis of seismo-acoustic data in volcanic environments. MISARA includes efficient algorithm implementations of well-established techniques for seismic and acoustic data analysis. It is designed to support

visualization, characterization, detection and location of volcano seismo-acoustic signals. Its intuitive, modular, structure facilitates rapid, semi-automated, inspection of data and results, thus reducing user effort. MISARA was tested using seismo-acoustic data recorded at Etna Volcano (Italy) in 2010, 2011 and 2019, and is intended for use in education and research, and to support routine data analysis at volcano observatories.

INTRODUCTION

Volcano seismology deals with a large variety of seismic and acoustic signals (e.g., McNutt et al., 2015). The analysis of these waveforms plays a key role in the surveillance of volcanoes and provides important insights on magmatic and hydrothermal processes in the plumbing system (e.g., Sparks et al., 2012; Chouet and Matoza, 2013; McNutt et al., 2015). The investigation of the wavefield properties of these signals and their source location is crucial for effective volcano monitoring. The application of traditional travel-time inversion methods to data from sparse networks, in particular to signals with emergent onsets such as Long Period (LP) or Very Long Period (VLP) earthquakes and volcanic tremor, is challenging. Owing to the nature of these signals, alternative localization methods have been used in recent years, including amplitude-based techniques (Di Grazia et al., 2006; Carbone et al., 2008; Cannata et al., 2013; Morioka et al., 2017) and array methods (e.g., Rost and Thomas, 2002).

Seismic and acoustic arrays consist of multiple sensors arranged in clusters on a spatial scale significantly shorter than the wavelength of interest. In array analysis, the waveforms recorded by each sensor are processed together based on the common waveform model of the signal (Aki and Richards, 1980). Depending on the wave propagation model (i.e., plane vs spherical wavefronts), a source location can be inferred directly or from back-propagation of the wave-vectors determined from the coherent wavefield propagation across the array (Havskov and Alguacil, 2016). Several studies have employed array techniques to investigate the evolution of seismic and acoustic sources during periods of volcanic unrest (Saccorotti et al., 2004; Di Lieto et al., 2007; Inza et al., 2014; Eibl et al., 2017; De Angelis et al., 2020), although their use as a monitoring tool remains limited (e.g., Coombs et al., 2018).

Over the past decade, the amount of seismic and acoustic monitoring data gathered on active volcanoes has grown tremendously, making their analysis a challenging task. At the same time, a plethora of software packages and algorithms for signal processing were developed in different programming environments, including the Python and Matlab platforms. The majority of these packages provide a broad range of command-line functionalities for the management and handling of waveform data and related metadata; examples include ObsPy (Beyreuther et al., 2010), SEIZMO (Euler, 2014) and GISMO (Thompson and Reyes., 2018). Other toolboxes were designed with a narrower focus on signal processing, including spectral analyses, and event detection and classification (e.g., Lesage, 2009; Messina and Langer, 2011; Bueno et al., 2020; Cortés et al., 2021). Finally, other packages were developed to specifically perform seismic array analyses (e.g., Pignatelli et al., 2008; Smith and Bean, 2020).

Here, we present MISARA (Matlab Interface for the Seismo-Acoustic aRary Analysis), a Matlab GUI that supports visualisation, detection and localization of volcano seismic and acoustic signals, with a focus on array techniques. In this manuscript, we will introduce the main features and functionalities of MISARA. We will demonstrate its use and showcase the capabilities of the software in analysing volcano seismic and acoustic waveforms, and discuss its suitability for both research and monitoring purposes.

OVERVIEW OF MISARA

MISARA is an open-source Matlab Interface developed to support users with the application of array techniques to seismic and acoustic signals. It is characterised by an intuitive and modular structure. MISARA is organised into different classes and modules, and its functionalities are accessed through several GUI windows (Fig. 1).

Home window

The Home window (Fig. 2) is the control panel of MISARA, which allows to manage all aspects of data processing, including the configuration of the data source, Input/Output options and the parametrization of all analyses that will be performed on the selected data. The Home panel includes four dynamic menus to independently manage, save and import settings from the last analysis performed, or to load a suite of default analysis parameters. It allows access to all other modules of MISARA for seismic and acoustic data processing.

Data preparation window

MISARA includes a module dedicated to the creation of appropriate data structures, that is the Create Dataset module (Fig. 3), which is accessed via the Data preparation window. MISARA works with seismic and acoustic waveforms archived as Matlab structure arrays, in a dedicated folder/file structure. These files contain the raw data and some relevant metadata (e.g., station name, sampling rate, timing of records, etc.). MISARA modules require two additional files, which contain Matlab structures providing the station coordinates and information on the instrument response, respectively.

The software can operate in two modes, depending on whether the data source is an off-line archive or a web-based data server. In the off-line mode, the user can read and convert common file formats into MISARA structures; these formats include the Seismic Analysis Code (SAC; Goldstein et al., 2003; Goldstein and Snoke, 2005), Standard for the Exchange of Earthquake Data (SEED/miniSEED) and DSS-Cube/Data-Cube3 file format (see DATA AND RESOURCES). In the other mode, the user can access data stored at the Incorporated Research Institutions for Seismology-Data Management Center (IRIS-DMC) via International Federation of Digital Seismograph Networks (FDSN) services (see DATA AND RESOURCES), to retrieve waveforms and station/channel metadata. The off-line mode allows to recover information from XML files (eXtensible Markup Language). However, when XML files are not available, it is still possible to manually input station coordinates and instrument response parameters.

MISARA modules

All modules of MISARA share a similar design and workflow. All analysis and visualization parameters can be customized (Fig. 4). The Data Pre-processing modules (Fig. 1) are designed to perform data quality checks, and to deconvolve the instrument response from the raw seismograms similarly to other Matlab codes (e.g., Haney et al., 2012; Thompson and Reyes., 2018). For seismic and acoustic array analyses, the Data Pre-processing modules also allow the user to evaluate the array response function using the Beam Pattern algorithm of Capon (1969). The Signal Features modules (Fig. 1) adopt well-established routines and algorithms for seismic and acoustic signal processing, such as spectrograms (Schlindwein et al., 1995) and coherograms (Welch, 1967), Root Mean Square (RMS; Kenney and Keeping, 1962), polarization analysis (Jurkevics, 1988), Short

Term Average/Long Term Average (STA/LTA; Allen, 1978) and the Sub-band Automatic LP Events Detection (SALPED; Garcia et al., 2017).

The Array modules (Fig. 1) implement several array processing algorithms for source localization of seismic and acoustic signals. This tool includes the Zero Lag Cross correlation analysis (ZLC; Frankel et al., 1991), MUltiple SIgnal Classification (MUSIC; Schmidt, 1986) algorithm, Semblance and Radial Semblance methods (Almendros et al., 2002). For the evaluation of uncertainties in the estimate of the source position, we have implemented the JackKnife method (Efron, 1982). Additional details on all MISARA utilities are available in the help section of the software and the detailed user manual included in the public release of the software (https://doi.org/10.5281/zenodo.7410076).

EXAMPLES

Here, we demonstrate the use and performances of MISARA through application to three cases studies. First, we perform analysis of volcanic tremor recorded by a seismic array deployed at Mt. Etna (Italy) in 2011 during intense lava fountain activity from its New South East Crater (NSEC). Second, we demonstrate the location of LP and VLP earthquakes recorded by the Mt. Etna permanent seismic network in 2010, which accompanied explosive activity at the Bocca Nuova crater (BN). Finally, we show the analysis the infrasound data recorded by an infrasound array deployed at Mt. Etna in 2019, when the NSEC crater produced intense Strombolian activity. Detailed instructions on how to use of MISARA to reproduce the analyses shown here are available consulting the user manual and the video tutorials provided with the latest software release.

Case study 1: Mt. Etna, 2011-seismic array

MISARA was tested using off-line data from a small-aperture seismic array deployed at Mt. Etna, Italy. The software configuration and its performances are summarized in Table A1. For this test, we used the Beam Pattern module to display the location of the array (Fig. 5a), its geometry (Fig. 5b), and to evaluate its response function at a selected target frequency (Fig. 5c). The array consisted of five single-component seismometers with an aperture of approximately 200 m, deployed at about 1 km from NSEC. Figure 5c, suggests that the configuration of the array allows reliable array analyses in the frequency band 1-3.0 Hz, which coincides with the dominant energy of volcanic tremor at Etna Volcano (e.g., Cannata et al., 2010). We note that the array has poor resolution at low frequencies (0.5 Hz) caused by a signal wavelength larger than its aperture. On the other hand, the sensitivity and resolution of the array is appropriate to investigate signals at frequencies up to 3 Hz. Aliasing becomes prevalent above 3 Hz.

The spectral features and source location of volcanic tremor were investigates using the Spectrogram and ZLC modules, respectively. An example of analysis of volcanic tremor, recorded during a lava fountain episode on 30 July, 2011 at NSEC, is shown in Figure 6. The results include time series of back-azimuth, ray parameter, tremor amplitude (RMS) and spectrogram linked to changes in eruptive activity. Significant variations in amplitude, frequency content and source location of tremor preceded and accompanied the onset of paroxysmal activity, which corresponded to shifts in the style and location of activity across different craters in the summit area of Mt. Etna (e.g., Patané et al., 2013; Moschella et al., 2018). Fig. 6a shows back-azimuths dominantly between -15°N and 5°N until about 7:00 am (UTC) on 30 July, pointing towards the NNE sector of Mt. Etna (Fig. 6f); between 7:00 and 8:00 am (UTC), which is twelve hours before the onset of lava fountain activity, the back-azimuth gradually migrated to 30-50°N (Fig. 6a), corresponding to the NSEC direction (Fig. 6f).

Case study 2: Mt. Etna, 2010-permanent seismic network

We also show the results of using MISARA with data recorded by the permanent seismic network operated by the Istituto Nazionale di Geofisica e Vulcanologia (INGV). We used signals recorded by seven stations deployed in the summit area of Mt. Etna (see Fig. 8 for station locations). These stations consisted of three-component, Trillium 40-s, seismometers (Nanometrics^{TM}) recording at a sampling rate of 100 Hz. An overview of the configuration and software performance for this case study is shown in Table A2. By using the STA/LTA and SALPED modules, we automatically detected LP and VLP events on 23 October, 2010 (Fig. 7), when the BN crater produced moderate-to-intense Strombolian activity. We selected events based on their features, such as frequency content (Fig. 7a), characteristic waveform (Fig. 7b) and particle motion of the signals (Fig. 7c).

Under the assumption of a homogeneous and isotropic propagation medium (wave velocity of 1.6 km/s), and thus of spherical wavefronts, we used the Semblance and Radial Semblance methods to track the source location of LP and VLP events, respectively. These two methods, based on waveform stacking, are similar to back-projection (Haney et al., 2014). Unlike back-projection, the Semblance method achieves the best performances on the radial components of the wavefield, while Radial Semblance cannot be applied to non-radial components of the wavefield (Almendros et al., 2002). We employed a grid-search approach using the signals recorded by seven INGV stations deployed in the summit area of Mt. Etna (Fig. 8). The results of our analyses are shown in Fig. 8. LP (Fig. 8a) and VLP (Fig. 8b) events were located below the BN crater at shallow depths, a common occurrence at Mt. Etna (e.g., Saccorotti et al., 2007; Cannata et al., 2009; Patanè et al., 2013; Zuccarello et al., 2013).

Case study 3: Mt. Etna, 2019- Infrasound array

MISARA was also tested using data from a small-aperture infrasound array deployed at Mt. Etna in 2019. The data used here were already analysed in De Angelis et al. (2020). The reader is refereed to this publication for additional information on this dataset. In particular, we focused on the infrasound waveforms recorded on 19th July, 2019, when the NSEC produced intense explosive activity. We configured MISARA to mimic the analysis in De Angelis et al. (2020). A brief summary on the parameters configuration and performances of MISARA for this case study is shown in Table A3.

An example of analysis of these data with MISARA is shown in Figure 9. We used the Spectrogram and ZLC modules to evaluate the main features and source position of the infrasound signal. The results of the analysis in Figure 9 are in agreement with De Angelis et al. (2020). In particular, Fig. 9a shows back-azimuths focused on 60°N, pointing towards the NSEC (Fig. 9e), as well as an increase in infrasound amplitude during the intensification of explosive activity (Figs. 9b,c, and d).

CONCLUSIONS

We have presented MISARA, an open-source Matlab-based GUI designed to perform analyses of seismic and acoustic waveform data. A suite of well-established algorithms for volcano seismic and acoustic signal processing have been integrated into the GUI, with a focus on array techniques. We note that although MISARA was developed to facilitate the analysis of seismic and acoustic signals in volcanic environments, it can be used for other research purposes.

The modular structure of MISARA (Fig. 1), offers the flexibility to easily integrate additional functionalities. Most data processing tasks in MISARA are automated, reducing user's errors and efforts. All processing parameters can be modified directly from within each module (Fig. 4), easily allowing multiple analyses on the same dataset. The modular structure offers input/output flexibility (Fig. 4).

Efficient algorithms with low computational cost are key for real-time or quasi real-time analyses of large amounts of data. Although MISARA does not currently support real-time data processing, its algorithm implementation meets the requirements for monitoring applications (e.g., Chao et al., 2017; Smith and Bean, 2020). Using a laptop with intermediate-to-high specifications (8 cores, 2.90 GHz Intel(R) Core (TM) i7-10700 CPU, 16GB RAM), the processing times for the test cases (Tables A1 and A2; Fig. A1) are of the order of few seconds to minutes for 1 day of data.

The software is suitable for applications including academic research, teaching and analysis of data from temporary deployments. Future developments will support the use of MISARA for operational purposes. While MISARA offers a user-friendly interface for the analysis of seismic and acoustic data from network and arrays, we acknowledge some possible limitations. For example, data pre-formatting routines in MISARA provide an alternative to the Python-based input and pre-processing procedures described in ObsPy (Beyreuther et al., 2010). In its current configuration, MISARA allows uploading data in a fast and clear manner, avoiding the repetition of any pre-processing routine in different modules of the software, or overloading the working memory. However, these routines could lead to duplication of data to the detriment of the storage requirements.

Future work to improve the capabilities of MISARA will be aimed at: (*i*) further simplifying the design and the structure of the software, providing an even more user-friendly GUI; (*ii*) fully automate every stage of data input and processing ; (*iii*) implementing additional methods for more a more comprehensive investigation of seismic and acoustic data (e.g., De Barros et al., 2011; Zuccarello et al., 2016; Montesinos et al., 2021); (*iv*) adapting the GUI for real-time data processing and the exploitation of data streams provided by web services (e.g., Smith and Bean, 2020); (*v*) integrating the GUI with well-established python libraries, such as ObsPy (Beyreuther et al., 2010).

DATA AND RESOURCES

MISARA, its user's manual, and test data can be downloaded at the URL: https://doi.org/10.5281/zenodo.7410076. The seismic and infrasound data used in this article were obtained from Istituto Nazionale di Geofisica e Vulcanologia, Osservatorio Etneo-Sezione di Catania (https://www.ct.ingv.it/). The commercial platform, MATLAB, is from Mathworks, available at http://www.mathworks.com. A MATLAB script to download the Incorporated Research Institutions for Seismology (IRIS) seismic data archive can be found at https://ds.iris.edu/ds/nodes/dmc/manuals/irisfetchm/. For the management of the DSS-Cube/Data-Cube3 files, gipptools package is available at https://www.gfz-potsdam.de/en/section/geophysical-imaging/infrastructure/geophysical-instrument-pool-potsdam-gipp/software/gipptools/. Additional details on SAC and SEED formats are available at http://www.iris.edu/manuals/.

ACKNOWLEDGEMENTS

L. Zuccarello is supported by the project SINFONIA, progetto Bando Ricerca Libera 2021 Delibera 214/2021-INGV, and by by the INGV Pianeta Dinamico 2021 Tema 8 SOME project (grant no. CUP D53J1900017001) funded by the Italian Ministry of University and Research "Fondo finalizzato al rilancio degli investimenti delle amministrazioni centrali dello Stato e allo sviluppo del Paese, legge 145/2018". S. De Angelis is supported by NERC grant NE/W004771/1. The authors thank the seismological technical staff of the Istituto Nazionale di Geofisica e Vulcanologia, Osservatorio Etneo-Sezione di Catania, for their support in the acquisition of seismic data.

REFERENCES

- Aki K. and P. G. Richards (1980). Quantitative seismology, *WH Freeman*, San Francisco, doi: 10.1002/gj.3350160110.
- Allen, R. V. (1978). Automatic earthquake recognition and timing from single traces, *Bulletin of the seismological society of America*, 68(5), 1521-1532, doi: 10.1785/BSSA0680051521.
- Allstadt, K. E., R. S. Matoza, A. B. Lockhart, S. C. Moran, J. Caplan-Auerbach, M. M. Haney, A. T. Thelen and S. D. Malone (2018). Seismic and acoustic signatures of surficial mass movements at volcanoes, *Journal of Volcanology and Geothermal Research,* 364, 76-106, doi: 10.1016/j.jvolgeores.2018.09.007.
- Almendros, J., B. Chouet, P. Dawson, and T. Bond (2002). Identifying elements of the plumbing system beneath Kilauea Volcano, Hawaii, from the source locations of very-long-period signals, *Geophysical Journal International*, 148(2), 303-312, doi: 10.1046/j.1365-246X.2002.01629.x.
- Almendros, J. and B. Chouet (2003). Performance of the radial semblance method for the location of very long period volcanic signals, *Bulletin of the Seismological Society of America,* 93(5), 1890-1903, doi: 10.1785/0120020143.
- Álvarez, I., L. García, S. Mota, G. Cortés, C. Benítez, and Á. De la Torre (2013). An automatic P-phase picking algorithm based on adaptive multiband processing, *IEEE*

Geoscience and remote sensing letters, 10(6), 1488-1492, doi:10.1109/LGRS.2013.2260720.

- Beyreuther, M., R. Barsch, L. Krischer, T. Megies, Y. Behr, and J. Wassermann (2010). ObsPy: A Python toolbox for seismology, *Seismological Research Letters*, 81(3), 530-533, doi: 10.1785/gssrl.81.3.530.
- Bueno, A., C. Benitez, S. De Angelis, A. D. Moreno, and J. M. Ibáñez (2019). Volcano-seismic transfer learning and uncertainty quantification with Bayesian neural networks, *IEEE Transactions on Geoscience and Remote Sensing*, 58(2), 892-902. doi: 10.1109/TGRS.2019.2941494.
- Bueno, A., L. Zuccarello, A. D. Moreno, J. Woollam, M. Titos, C. Benítez, I. Álvarez, J. Prudencio and S. De Angelis (2020). PICOSS: Python interface for the classification of seismic signals, *Computers & geosciences*, 142, doi: 10.1016/j.cageo.2020.104531.
- Cannata, A., M. Hellweg, G. Di Grazia, S. Ford, S. Alparone, S. Gresta, P. Montalto and D. Patanè (2009). Long period and very long period events at Mt. Etna volcano: Characteristics, variability and causality, and implications for their sources, *Journal of Volcanology and Geothermal Research*, 187(3-4), 227-249, doi:10.1016/j.jvolgeores.2009.09.007.
- Cannata, A., G. Di Grazia, P. Montalto, F. Ferrari, G. Nunnari, D. Patanè, D., and E. Privitera (2010). New insights into banded tremor from the 2008–2009 Mount Etna eruption, *Journal of Geophysical Research: Solid Earth*, 115(B12), doi:10.1029/2009JB007120.

- Cannata, A., G. Di Grazia, M. Aliotta, C. Cassisi, P. Montalto, and D. Patanè (2013). Monitoring seismo-volcanic and infrasonic signals at volcanoes: Mt. Etna case study, *Pure and Applied Geophysics*, 170(11), 1751-1771, doi:10.1007/s00024-012-0634 x.
- Carbone, D., L. Zuccarello, and G. Saccorotti (2008). Geophysical indications of magma uprising at Mt Etna during the December 2005 to January 2006 non-eruptive period, *Geophysical Research Letters*, 35(6), doi: 10.1029/2008GL033212.
- Chao, W. A., Y. M. Wu, L. Zhao, H. Chen, Y. G. Chen, J. M. Chang, and C. M. Lin (2017). A first near real-time seismology-based landquake monitoring system, *Scientific reports*, 7(1), 1-12, doi: 10.1038/srep43510.
- Chouet, B. A., and R. S. Matoza (2013). A multi-decadal view of seismic methods for detecting precursors of magma movement and eruption, *Journal of Volcanology and Geothermal Research,* 252, 108-175, doi: 10.1016/j.jvolgeores.2012.11.013.
- Coombs, M. L., A. G. Wech, M. M. Haney, J. J. Lyons, D. J. Schneider, H. F. Schwaiger, K. L. Wallace, D. Fee, J. T. Freymueller, J. R. Schaefer, and G. Tepp (2018). Short-term forecasting and detection of explosions during the 2016–2017 eruption of Bogoslof volcano, Alaska, *Frontiers in Earth Science*, 6, 122, doi:10.3389/feart.2018.00122.
- Cortés, G., R. Carniel, P. Lesage, M. Á. Mendoza, and I. Della Lucia (2021). Practical volcano-independent recognition of seismic events: VULCAN. ears project, *Frontiers in Earth Science*, 8, 616676, doi:10.3389/feart.2020.616676.
- De Angelis, S., M. M. Haney, J. J. Lyons, A. Wech, D. Fee, A. Diaz-Moreno, and L. Zuccarello (2020). Uncertainty in detection of volcanic activity using infrasound arrays:

examples from Mt. Etna, Italy, *Frontiers in Earth Science*, 8, 169, doi: 10.3389/feart.2020.00169.

- De Angelis, S., L. Zuccarello, S. Rapisarda and V. Minio (2021). Introduction to a community dataset from an infrasound array experiment at Mt. Etna, Italy, *Scientific Data*, 8(1), 1-9, doi: 10.1038/s41597-021-01030-6.
- De Barros, L., I. Lokmer, C. J. Bean, G. S. O'Brien, G. Saccorotti, J. P. Métaxian, L. Zuccarello, and D. Patanè (2011). Source mechanism of long-period events recorded by a high-density seismic network during the 2008 eruption on Mount Etna, *Journal of Geophysical Research: Solid Earth*, 116(B1), doi: 10.1029/2010JB007629.
- Diaz-Moreno, A., A. Roca, A. Lamur, B. H. Munkli, T. Ilanko, T. D. Pering, A. Pineda, and S. De Angelis (2020). Characterization of acoustic infrasound signals at Volcán de Fuego, Guatemala: a baseline for volcano monitoring, *Frontiers in Earth Science*, 8, 549774, doi: 10.3389/feart.2020.549774.
- Di Grazia, G., S. Falsaperla, and H. Langer (2006). Volcanic tremor location during the 2004 Mount Etna lava effusion, *Geophysical research letters*, 33(4), doi:10.1029/2005GL025177.
- Di Lieto, B., G. Saccorotti, L. Zuccarello, M. L. Rocca, and R. Scarpa (2007). Continuous tracking of volcanic tremor at Mount Etna, Italy, *Geophysical Journal International*, 169(2), 699-705, doi: 10.1111/j.1365-246X.2007.03316.x.
- Efron, B. (1982). The jackknife, the bootstrap and other resampling plans, *Society for industrial and applied mathematics*, doi: 10.1137/1.9781611970319.

- Eibl, E. P., C. J. Bean, K. S. Vogfjörd, Y. Ying, I. Lokmer, M. Möllhoff, G. S. O'Brien, and F. Pálsson (2017). Tremor-rich shallow dyke formation followed by silent magma flow at Bárðarbunga in Iceland, *Nature Geoscience*, 10(4), 299-304, doi:10.1038/ngeo2906.
- Euler, G. (2014). Project SEIZMO, Available at: http://epsc.wustl.edu/~ggeuler/codes/m/seizmo/.
- Evita, M., A. Zakiyyatuddin, S. Seno, N. S. Aminah, W. Srigutomo, I. Meilano, A. Setiawan, H. Darmawan, I. Suyanto, Irzaman, M. Yasin, Perdinan, R. Apsari, Wahyudi, W. Suryanto, and M. Djamal (2021). Development of Volcano Warning System for Kelud Volcano, *Journal of Engineering and Technological Sciences*, 53(2), 210202, doi: 10.5614/j.eng.technol.sci.2021.53.2.2.
- Frankel, A., S. Hough, P. Friberg, and R. Busby (1991). Observations of Loma Prieta aftershocks from a dense array in Sunnyvale, California, *Bulletin of the seismological Society of America*, 81(5), 1900-1922, doi: 10.1785/BSSA0810051900.
- Garcıa, L., I. Alvarez, M. Titos, A. D. Moreno, M. C. Benıtez, and A. de la Torre (2017). Automatic detection of long period events based on subband-envelope processing, *IEEE Journal of Selected Topics in Applied Earth Observations and Remote Sensing*, 10(11), 5134-5142, doi: 10.1109/jstars.2017.2739690.
- Giudicepietro, F., C. López, G. Macedonio, S. Alparone, F. Bianco, S. Calvari, W. De Cesare, D. Delle Donne, B. Di Lieto, A. M. Esposito, M. Orazi, R. Peluso, E. Privitera, P. Romano, G. Scarpato and A. Tramelli (2020). Geophysical precursors of the July-August 2019 paroxysmal eruptive phase and their implications for Stromboli volcano (Italy)

monitoring, *Scientific reports*, 10(1), 1-16, doi: https://doi.org/10.1038/s41598-020-67220-1.

- Goldstein, P., D. Dodge, M. Firpo, L. Minner, W. Lee, H. Kanamori, P. Jennings, and C. Kisslinger (2003). SAC2000: Signal processing and analysis tools for seismologists and engineers, invited contribution to *The IASPEI International Handbook of Earthquake and Engineering Seismology*, Edited by WHK Lee, H. Kanamori, P.C. Jennings, and C. Kisslinger, Academic Press, London.
- Goldstein, P., and A. Snoke, (2005), SAC Availability for the IRIS Community, *Incorporated Research Institutions for Seismology Newsletter*, 7(UCRL-JRNL-211140), doi: https://www.osti.gov/servlets/purl/875360i
- Haney, M. M., J. Power, M. West, P. Michaels (2012). Causal Instrument Corrections for Short-Period and Broadband Seismometers, *Seismological Research Letters*; 83 (5): 834–845, doi: 10.1785/0220120031.
- Haney, M. M. (2014). Backprojection of volcanic tremor, *Geophysical Research Letters*, 41, 1923- 1928, doi:10.1002/2013GL058836.
- Havskov, J., and G. Alguacil (2016). Seismic Arrays, In *Instrumentation in Earthquake Seismology* (pp. 309-329), Springer, Cham, doi: 10.1007/978-3-319-21314-9_9.
- Inza, L. A., J. P. Métaxian, J. I. Mars, C. J. Bean, G. S. O'Brien, O. Macedo, and D. Zandomeneghi (2014). Analysis of dynamics of vulcanian activity of Ubinas volcano, using multicomponent seismic antennas, *Journal of Volcanology and Geothermal Research*, 270, 35-52., doi: 10.1016/j.jvolgeores.2013.11.008.

- Jousset, P., A. Budi-Santoso, A. D. Jolly, M. Boichu, Surono, S. Dwiyono, S. Dwiyono, S.Sumarti, S. Hidayati, and P. Thierry (2013). Signs of magma ascent in LP and VLP seismic events and link to degassing: an example from the 2010 explosive eruption at Merapi volcano, Indonesia, *Journal of Volcanology and Geothermal Research*, 261, 171-192, doi: 10.1016/j.jvolgeores.2013.03.014.
- Jurkevics, A. (1988). Polarization analysis of three-component array data, *Bulletin of the seismological society of America*, 78(5), 1725-1743, doi: 10.1785/BSSA0780051725.
- Kenney, J. F., and E. S. Keeping (1962). Root Mean Square, in *Mathematics of Statistics*, Pt. 1, 3rd ed. Princeton, NJ: Van Nostrand, pp. 59-60, 1962.
- Lehr, J., F. Eckel, M. Thorwart, W. and Rabbel (2019). Low-Frequency Seismicity at Villarrica Volcano: Source Location and Seismic Velocities, *Journal of Geophysical Research: Solid Earth*, 124(11), 11505-11530, doi: 10.1029/2018JB017023.
- Lesage, P. (2009). Interactive Matlab software for the analysis of seismic volcanic signals, *Computers & Geosciences*, 35(10), 2137-2144, doi: 10.1016/j.cageo.2009.01.010.
- Li, L., D. Becker, H. Chen, X. Wang, and D. Gajewski (2018). A systematic analysis of correlation-based seismic location methods, *Geophysical Journal International*, 212(1), 659-678, doi: 10.1093/gji/ggx436.
- McKee, K., D. Fee, A. Yokoo, R. S. Matoza, and K. Kim (2017). Analysis of gas jetting and fumarole acoustics at Aso Volcano, Japan, *Journal of Volcanology and Geothermal Research*, 340, 16-29, doi: 10.1016/j.jvolgeores.2017.03.029.

- McNutt, S. R., G. Thompson, M. E. West, D. Fee, S. Stihler, and E. Clark, (2013). Local seismic and infrasound observations of the 2009 explosive eruptions of Redoubt Volcano, Alaska, *Journal of Volcanology and Geothermal Research*, 259, 63-76., doi: 10.1016/j.jvolgeores.2013.03.016.
- McNutt, S. R., G. Thompson, J. Johnson, S. De Angelis, and D. Fee (2015). Seismic and infrasonic monitoring, In *The encyclopedia of volcanoes* (pp. 1071-1099), Academic Press., doi: 10.1016/B978-0-12-385938-9.00063-8.
- Messina, A., and H. Langer (2011). Pattern recognition of volcanic tremor data on Mt. Etna (Italy) with KKAnalysis—A software program for unsupervised classification, *Computers & Geosciences*, 37(7), 953-961, doi: 10.1016/j.cageo.2011.03.015.
- Montesinos, B. M., C. J. Bean, and I. Lokmer (2021). Quantifying strong seismic propagation effects in the upper volcanic edifice using sensitivity kernels, *Earth and Planetary Science Letters*, 554, doi: 10.1016/j.epsl.2020.116683.
- Morioka, H., H. Kumagai, and T. Maeda (2017). Theoretical basis of the amplitude source location method for volcano-seismic signals, *Journal of Geophysical Research: Solid Earth*, 122(8), 6538-6551, doi:10.1002/2017JB013997.
- Moschella, S., A. Cannata, G. Di Grazia, and S. Gresta (2018). Insights into lava fountain eruptions at Mt. Etna by improved source location of the volcanic tremor, *Annals of Geophysics*, doi: 10.4401/ag-7552.
- Patanè, D., A. Aiuppa, M. Aloisi, B. Behncke, A. Cannata, M. Coltelli, G. Di Grazia, S. Gambino, S. Gurrieri, M. Mattia, and G. Salerno (2013). Insights into magma and fluid transfer at Mount Etna by a multiparametric approach: A model of the events leading to

the 2011 eruptive cycle, *Journal of Geophysical Research: Solid Earth*, 118(7), 3519-3539, doi: 10.1002/jgrb.50248.

- Pignatelli, A., A. Giuntini, and R. Console (2008). Matlab software for the analysis of seismic waves recorded by three-element arrays, *Computers & geosciences*, 34(7), 792-801, doi: 10.1016/j.cageo.2007.10.003.
- Ripepe, M., E. Marchetti, D. Delle Donne, R. Genco, L. Innocenti, G. Lacanna, and S. Valade (2018). Infrasonic early warning system for explosive eruptions, *Journal of Geophysical Research: Solid Earth*, 123(11), 9570-9585, doi: 10.1029/2018JB015561.
- Saccorotti, G., I. Lokmer, C. J. Bean, G. Di Grazia, and D. Patanè (2007). Analysis of sustained long-period activity at Etna Volcano, Italy, *Journal of volcanology and geothermal research*, 160(3-4), 340-354, doi: 10.1016/j.jvolgeores.2006.10.008.
- Schlindwein, V., J. Wassermann, and F. Scherbaum (1995). Spectral analysis of harmonic tremor signals at Mt. Semeru volcano, Indonesia, *Geophysical research letters*, 22(13), 1685-1688, doi: 10.1029/95GL01433.
- Schmidt, R. O. (1986). Multiple emitter location and signal parameter estimation, *IEEE Transactions on Antennas and Propagation*, 34, 276–280, doi: 10.1109/TAP.1986.1143830.
- Sciotto, M., A. Cannata, G. Di Grazia, and P. Montalto (2022). Volcanic tremor and long period events at Mt. Etna: Same mechanism at different rates or not?, *Physics of the Earth and Planetary Interiors*, 324, 106850, doi: 10.1016/j.pepi.2022.106850.

- Smith, P. J., and C. J. Bean (2020). RETREAT: A REal-Time TREmor Analysis Tool for Seismic Arrays, With Applications for Volcano Monitoring, *Frontiers in Earth Science*, 8, doi: 10.3389/feart.2020.586955.
- Sparks, R. S. J., J. Biggs, and J. W. Neuberg (2012). Monitoring volcanoes, *Science*, 335(6074), 1310-1311, doi:10.1126/science.1219485.
- Spina, R., A. Fornaia, and E. Tramontana(2020). VSEW: an early warning system for volcanic and seismic events, In *2020 IEEE International Conference on Smart Computing* (*SMARTCOMP*), 398-403, doi: 10.1109/SMARTCOMP50058.2020.00084.
- Sugimura, S., T. Nishimura, G. Lacanna, D. Legrand, S. Valade, and M. Ripepe (2021). Seismic Source Migration During Strombolian Eruptions Inferred by Very-Near-Field Broadband Seismic Network, *Journal of Geophysical Research: Solid Earth*, 126(12), doi: 10.1029/2021JB022623.
- Thompson, G., and C. Reyes (2018). GISMO-A Seismic Data Analysis Toolbox for MATLAB [software package], available at http:// geoscience community codes.github.io/GISMO/.
- Welch, P. (1967). The use of fast Fourier transform for the estimation of power spectra: a method based on time averaging over short, modified periodograms, *IEEE Transactions on audio and electroacoustics*, 15(2), 70-73, doi: 10.1109/TAU.1967.1161901.
- Zuccarello, L., M. R. Burton, G. Saccorotti, C. J. Bean, and D. Patanè (2013). The coupling between very long period seismic events, volcanic tremor, and degassing rates at Mount Etna volcano, *Journal of Geophysical Research: Solid Earth*, 118(9), 4910-4921, doi: 10.1002/jgrb.50363.

- Zuccarello, L., M. Paratore, M. La Rocca, F. Ferrari, A. Messina, S. Branca, D. Contrafatto, D. Galluzzo and S. Rapisarda (2016). Shallow velocity model in the area of Pozzo Pitarrone, Mt. Etna, from single station, array methods and borehole data, *Annals of Geophysics*, doi: 10.4401/ag-7086.
- Zuccarello, L., S. De Angelis, V. Minio, G. Saccorotti, C. J. Bean, M. Paratore, and J. Ibáñez (2022). Volcanic tremor tracks changes in multi-vent activity at MountEtna, Italy: Evidence from analyses of seismic array data, *Geophysical Research Letters*, 49, 2022GL100056, doi: 10.1029/2022GL100056.

FULL MAILING ADDRESS FOR EACH AUTHOR

Minio Vittorio - vittorio.minio@phd.unict.it

Zuccarello Luciano - luciano.zuccarello@ingv.it

De Angelis Silvio - silvioda@liverpool.ac.uk

Di Grazia Giuseppe - giuseppe.digrazia@ingv.it

Saccorotti Gilberto - gilberto.saccorotti@ingv.it

LIST OF FIGURE CAPTIONS

Figure 1. Overview of MISARA. a) Data preparation window, for data preparation and formatting. b) Home window, the main panel for management of all functionalities of MISARA. c) Data Pre-processing modules, for data quality control. d) Signal features modules, provide access to data processing including array, spectral, polarization, location and detection analysis. e) Array analysis modules, for source location methods based on multi-channel techniques.

Figure 2. Screenshot of the Home window, showing a selection of configurable input parameters, and access to modules for data formatting and analysis.

Figure 3. Screenshot of the Create Dataset module, showing the configurable parameters for conversion of Input files, creation of MISARA data structures and to retrieve waveforms and channel metadata.

Figure 4. Example of the generic structure of MISARA modules. a) Results plot panel; b) Data import panel; c) Panel for additional data selection or management of additional functionalities (for example, channel selection or error calculations); d) Panel for setup of temporary parameters that affects the current analyses and its output; e) Control panel for processes within the module, such as visualization of results, data and figure outputs. f) Text window, displaying any information about data processing including errors, warnings or command prompt messages.

Figure 5. Output from the Beam Pattern module for a seismic array deployed at Mt. Etna during 2011. a) Array location (red triangle) at Mt. Etna, East Sicily, Italy. b) Detail of array geometry

showing five sensors and an array aperture of ~200 m. All sensors are single-component Lennartz LE-3D/20s seismometers. c) Array response functions plotted at 0.5, 1.0, 2.0, 3.0, 4.0 and 5.0 Hz.

Figure 6. Output from the Signal viewer, Spectrogram and ZLC modules from analyses of volcanic tremor recorded on 30th July 2011 at Mt. Etna, Italy. a) Temporal evolution of the array-calculated backazimuth. The backazimuth ranges between -15°N and 5°N, during quiescent periods, and between 30°N and 50°N during eruptive activity. b) Temporal evolution of the seismic ray parameter. The parameter is observed to increase at the onset of eruptive activity from 0.6-1.0 s/km to 0.7-1.2 s/km, possibly indicating a source migrating at shallower depth. ZLC analysis was performed on data were filtered in the 1.0-1.5 Hz frequency band; a) and b) backazimuths calculated for data windows with array cross correlation coefficients greater than 0.75; c) 1-hour long moving average of RMS amplitudes in the 1.0-1.5 Hz frequency range at the central node of the array. d) Seismic signal at the central node of the array. e) Spectrogram at the central node of the array; f) Polar histogram of backazimuth results in (a) and plotted on the Digital Elevation Model of the summit area of Mt. Etna with the main craters (white circles; Bocca Nuova: BN; Voragine: VOR; North-East Crater: NEC; South-East Crater: SEC; New South-East Crater: NSEC). g) Bi-variate distribution (2D histogram) of ray parameter and back-azimuth shown in (a) and (b), respectively.

Figure 7. Examples of output from the SALPED and STA/LTA modules for detection and particle motion analyses of LP and VLP events recorded on 23rd October 2010 at ECPN station. a) Spectrograms of an example LP and VLP waveform and their waveform; c) Particle motion of the LP and VLP signals.

Figure 8. Examples of outputs of the Semblance and Radial Semblance modules for the analyses of LP and VLP events recorded on 23rd October 2010. Three sections of (a) Semblance and (b) Radial Semblance grids through the largest value node; the results shown are average distributions for 38 LPs (a) and 51 VLP (b), respectively; the grid of 5x5x2 km^3 (E-W, N-S and vertical directions) is interpolated to the Digital Elevation Model of Mt. Etna.

Figure 9. Output from the Signal viewer, Spectrogram and ZLC modules from analyses of infrasonic tremor recorded on 30th July 2011 at Mt. Etna, Italy. a) Temporal evolution of the array-calculated backazimuth, ranging between 50°N and 65°N. The ZLC analysis was performed on data were filtered in the 0.7-15 Hz frequency band. b) 1-hour long moving average of RMS amplitudes in the 0.7-15 Hz frequency range at the central node of the array. c) Infrasound signal at the central node of the array. d) Spectrogram at the central node of the array. e) Polar histogram of backazimuth results in (a) and plotted on the Digital Elevation Model of the summit area of Mt. Etna with the main craters (white circles; Bocca Nuova: BN; Voragine: VOR; North-East Crater: NEC; South-East Crater: SEC; New South-East Crater: NSEC). f) Bi-variate distribution (2D histogram) of ray parameter and backazimuth, respectively.

FIGURES

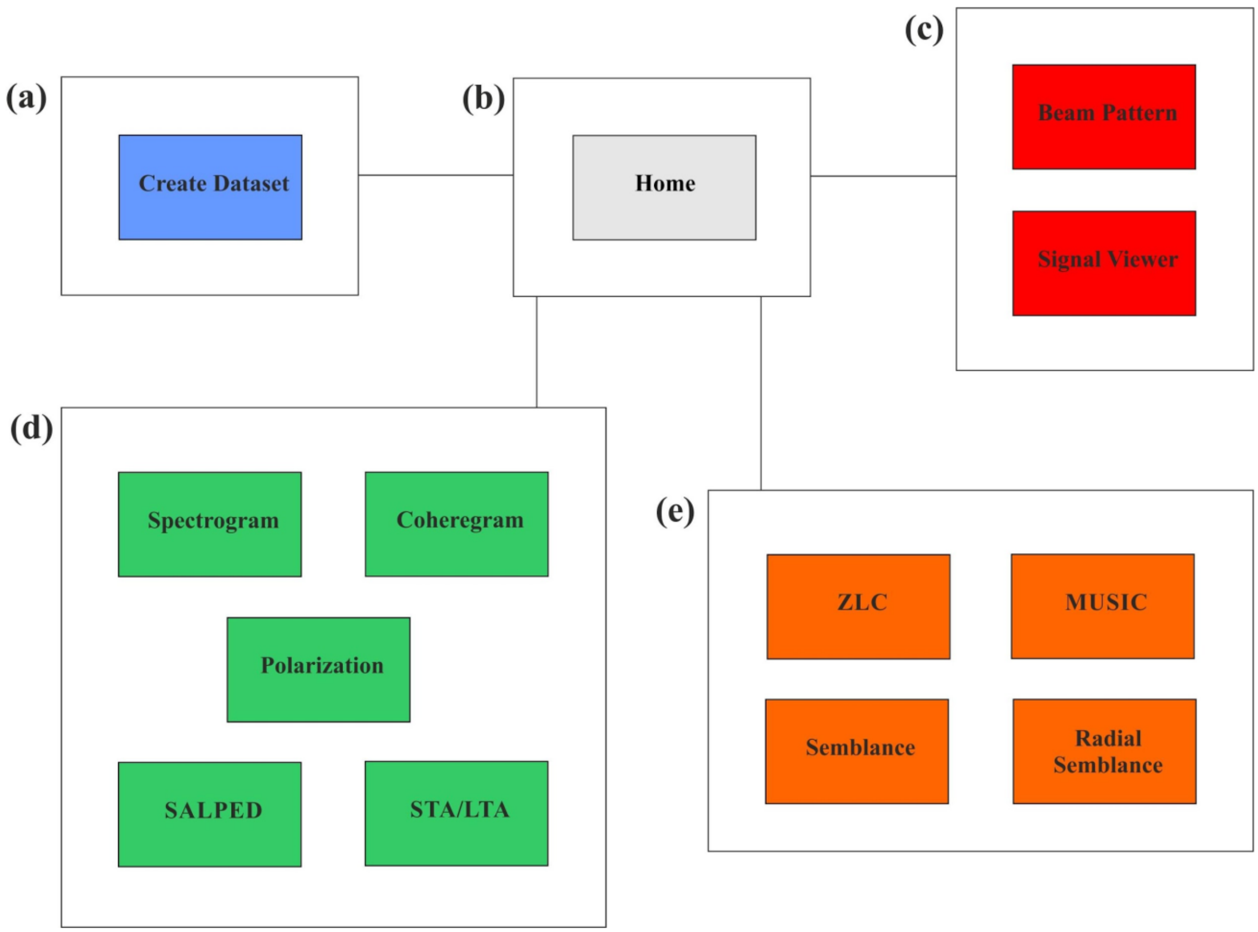

Figure 1. Overview of MISARA. a) Data preparation window, for data preparation and formatting. b) Home window, the main panel for management of all functionalities of MISARA. c) Data Pre-processing modules, for data quality control. d) Signal features modules, provide access to data processing including array, spectral, polarization, location and detection analysis. e) Array analysis modules, for source location methods based on multi-channel techniques.

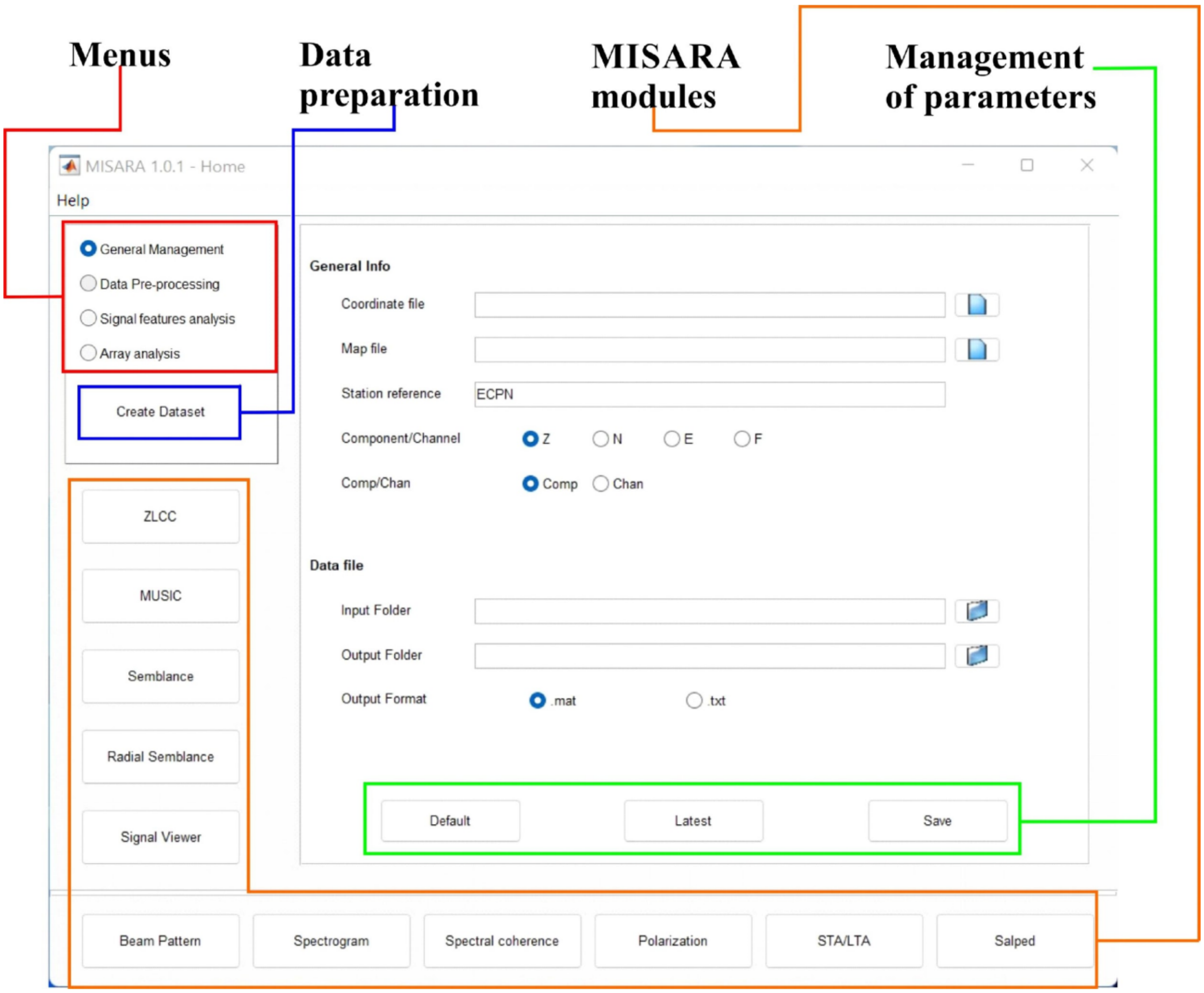

Figure 2. Screenshot of the Home window, showing a selection of configurable input parameters, and access to modules for data formatting and analysis.

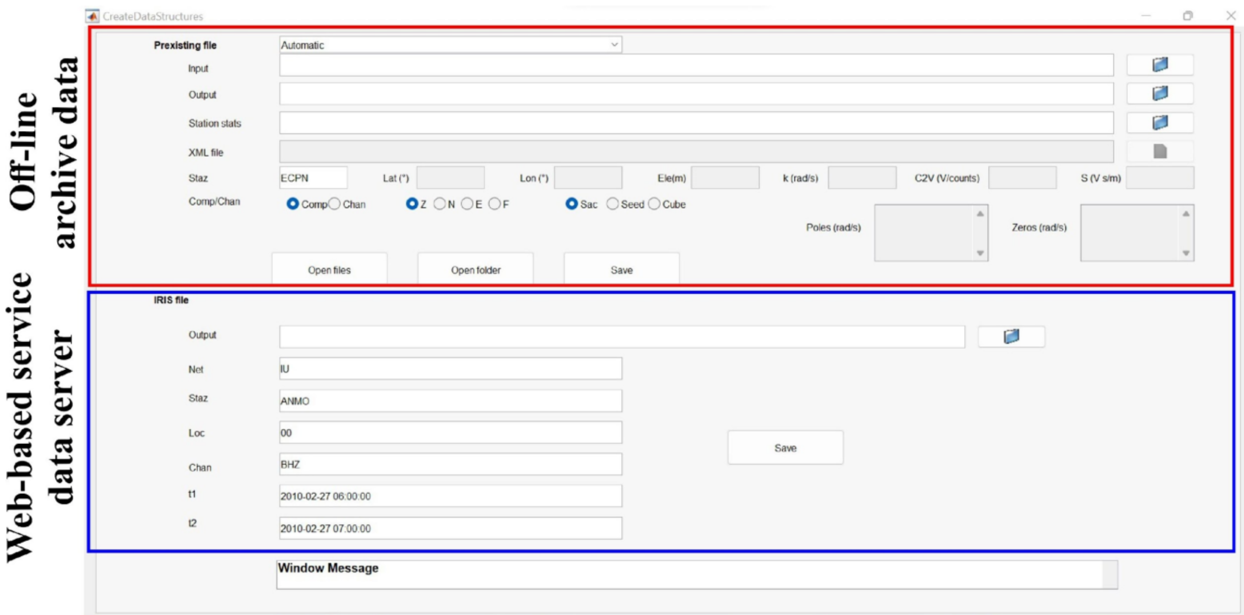

Figure 3. Screenshot of the Create Dataset module, showing the configurable parameters for conversion of Input files, creation of MISARA data structures and to retrieve waveforms and channel metadata.

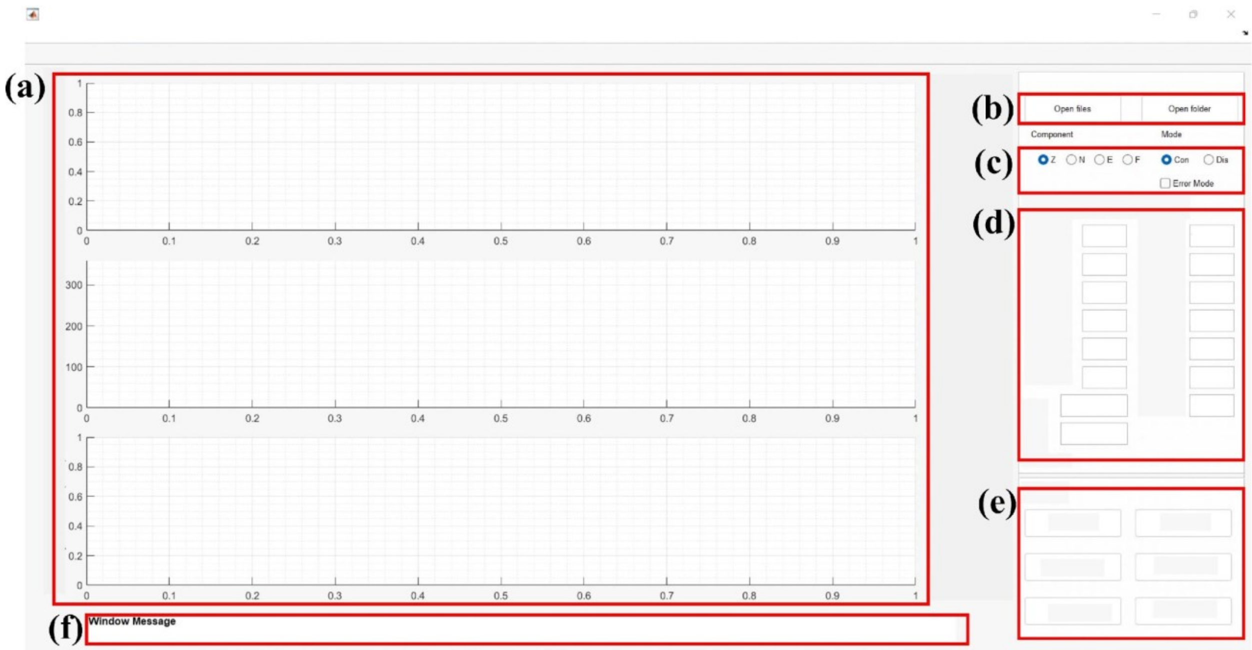

Figure 4. Example of the generic structure of MISARA modules. a) Results plot panel; b) Data import panel; c) Panel for additional data selection or management of additional functionalities (for example, channel selection or error calculations); d) Panel for setup of temporary parameters that affects the current analyses and its output; e) Control panel for processes within the module, such as visualization of results, data and figure outputs. f) Text window, displying any information about data processing including errors, warnings or command prompt messages.

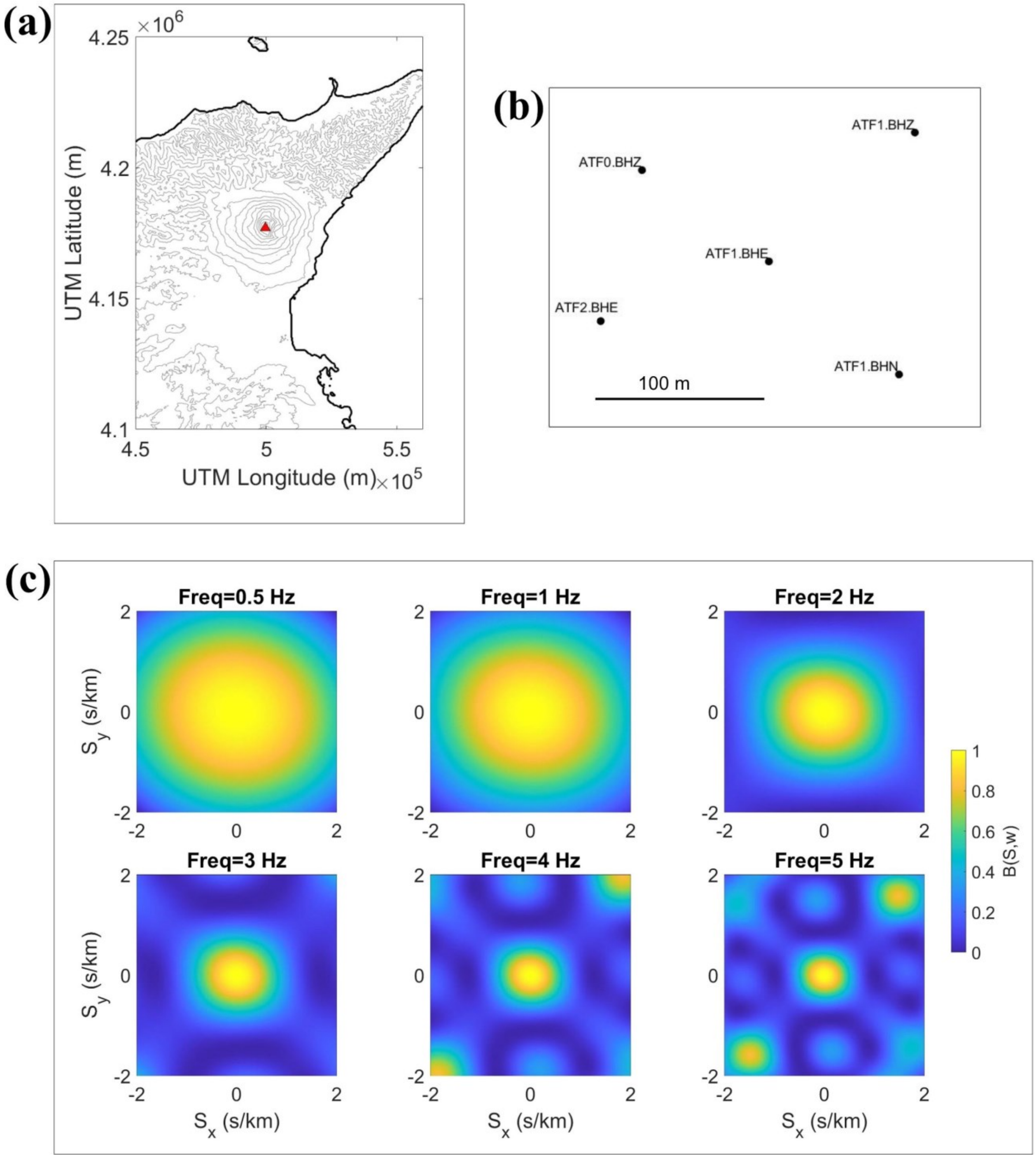

Figure 5. Output from the Beam Pattern module for a seismic array deployed at Mt. Etna during 2011. a) Array location (red triangle) at Mt. Etna, East Sicily, Italy. b) Detail of array geometry showing five sensors and an array aperture of ~200 m. All sensors are single-component Lennartz LE-3D/20s seismometers. c) Array response functions plotted at 0.5, 1.0, 2.0, 3.0, 4.0 and 5.0 Hz.

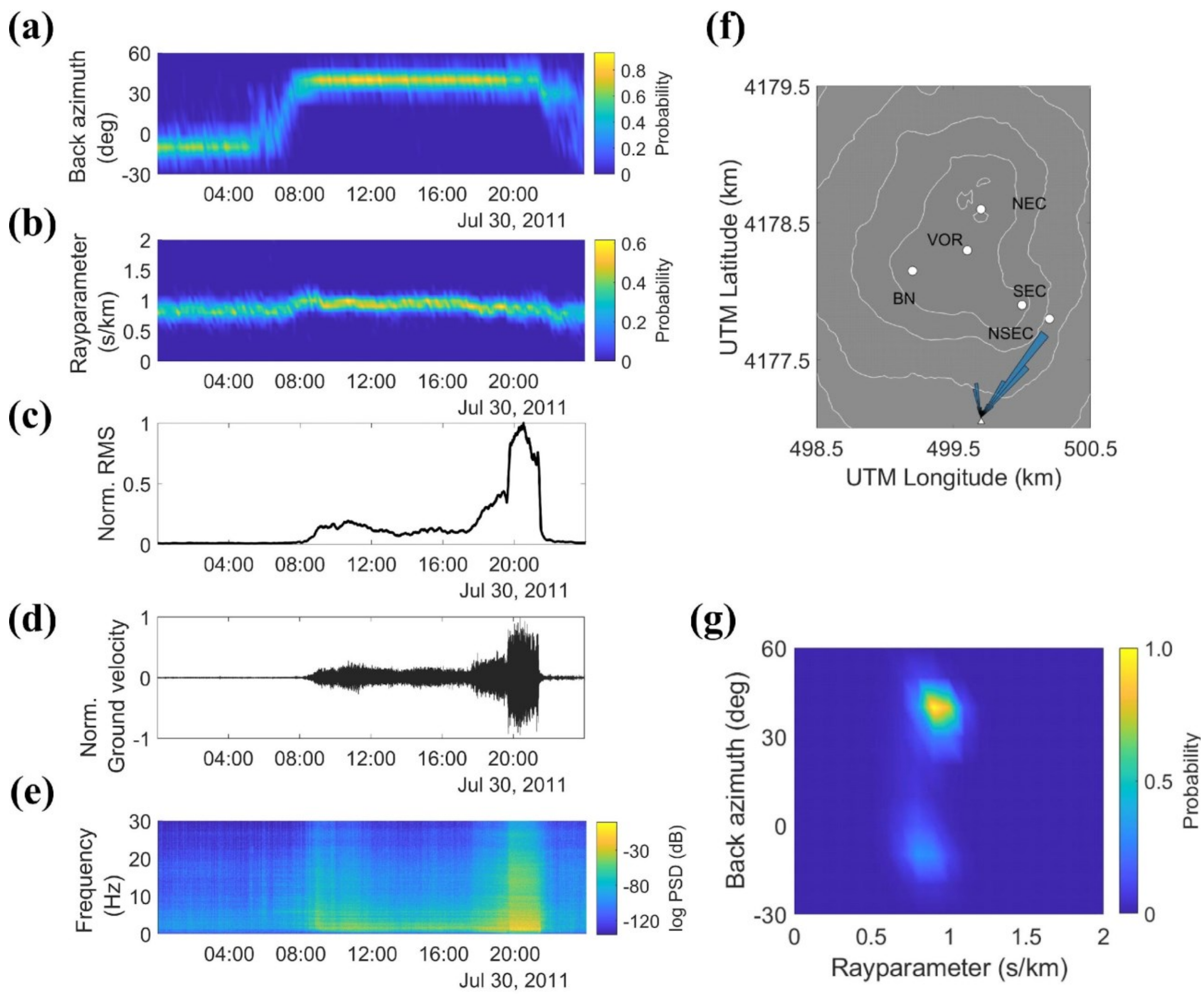

Figure 6. Output from the Signal viewer, Spectrogram and ZLC modules from analyses of volcanic tremor recorded on 30th July 2011 at Mt. Etna, Italy.. a) Temporal evolution of the array-calculated backazimuth. The backazimuth ranges between -15°N and 5°N, during quiescent periods, and between 30°N and 50°N during eruptive activity. b) Temporal evolution of the seismic ray parameter. The parameter is observed to increase at the onset of eruptive activity from 0.6-1.0 s/km to 0.7-1.2 s/km, possibly indicating a source migrating at shallower depth. ZLC analysis was performed on data were filtered in the 1.0-1.5 Hz frequency band; a) and b) backazimuths

calculated for data windows with array cross correlation coefficients greater than 0.75; c) 1-hour long moving average of RMS amplitudes in the 1.0-1.5 Hz frequency range at the central node of the array. d) Seismic signal at the central node of the array. e) Spectrogram at the central node of the array; f) Polar histogram of backazimuth results in (a) and plotted on the Digital Elevation Model of the summit area of Mt. Etna with the main craters (white circles; Bocca Nuova: BN; Voragine: VOR; North-East Crater: NEC; South-East Crater: SEC; New South-East Crater: NSEC). g) Bi-variate distribution (2D histogram) of ray parameter and back-azimuth shown in (a) and (b), respectively.

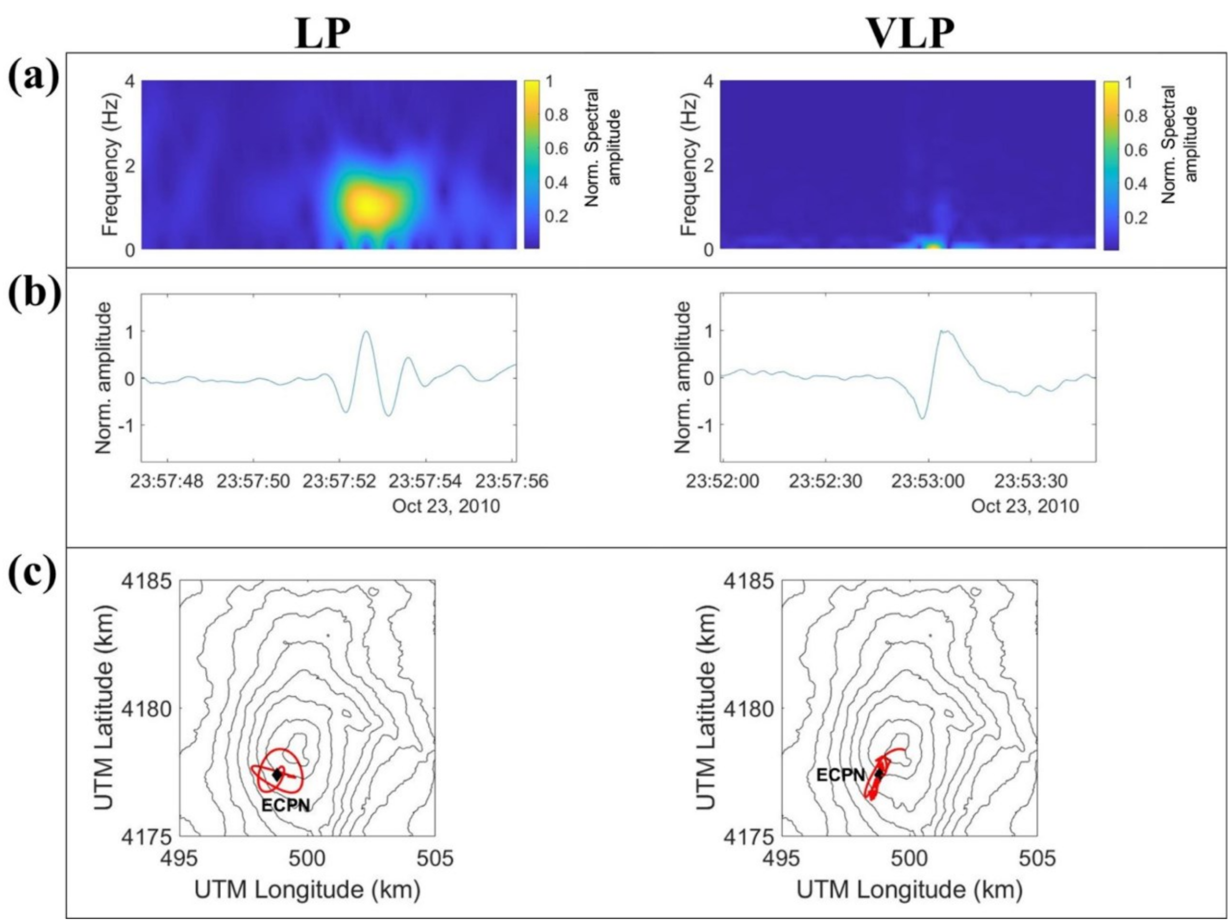

Figure 7. Examples of output from the SALPED and STA/LTA modules for detection and particle motion analyses of LP and VLP events recorded on 23rd October 2010 at ECPN station. a) Spectrograms of an example LP and VLP waveform and their waveform; c) Particle motion of the LP and VLP signals.

LP

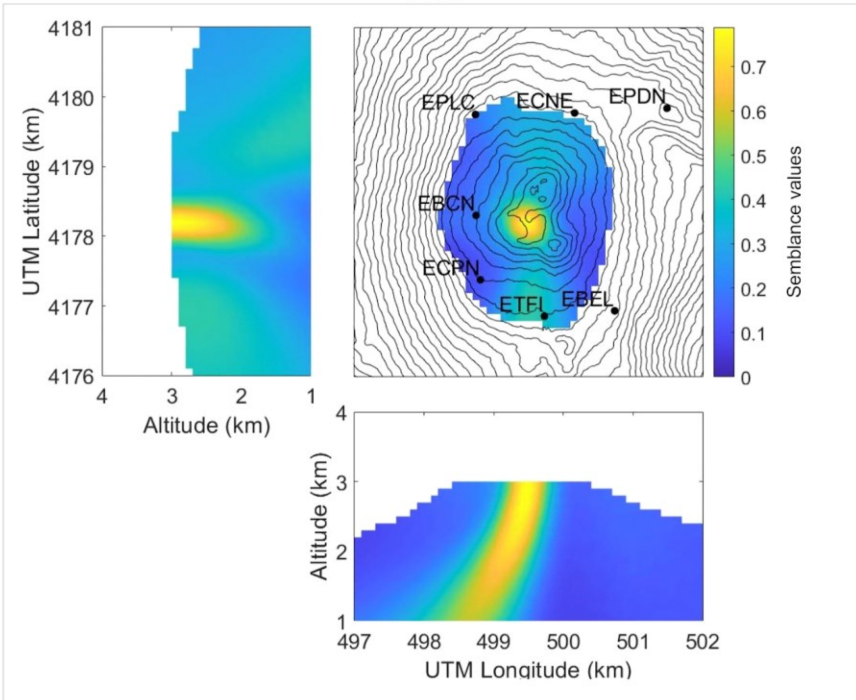
(a)
UTM Latitude (km)
4181
4180
4179
4178
4177
4176
4
3
2
1
Altitude (km)
EPLC
ECNE
EPDN
EBCN
ECPN
ETFL
EBEL
0.7
0.6
0.5
0.4
0.3
0.2
0.1
0
Semblance values
Altitude (km)
497
498
499
500
501
502
UTM Longitude (km)

VLP

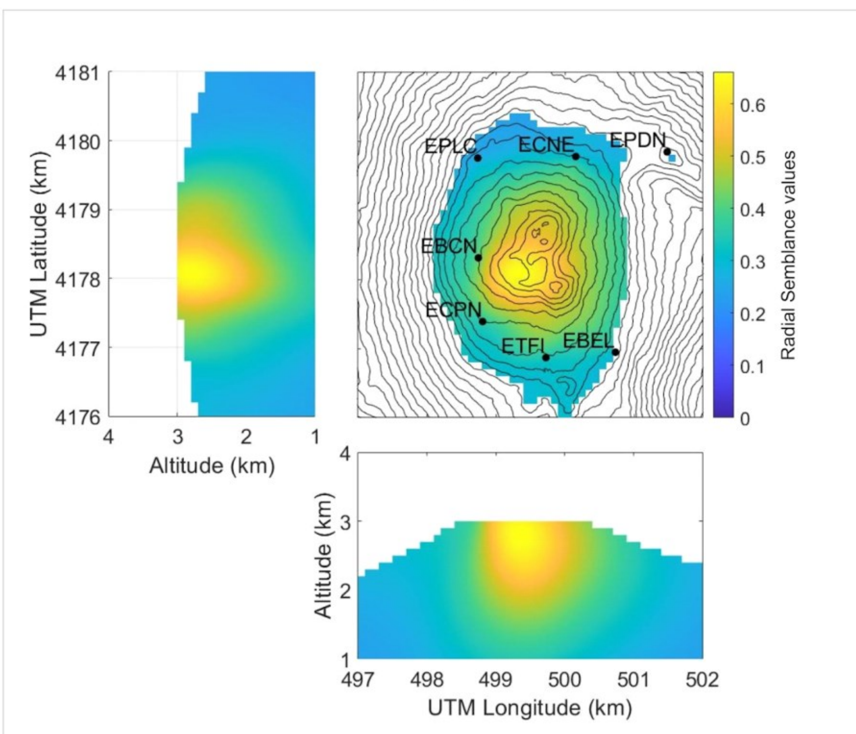
(b)
UTM Latitude (km)
4181
4180
4179
4178
4177
4176
4
3
2
1
Altitude (km)
EPLC
ECNE
EPDN
EBCN
ECPN
ETFL
EBEL
0.6
0.5
0.4
0.3
0.2
0.1
0
Radial Semblance values
Altitude (km)
497
498
499
500
501
502
UTM Longitude (km)

Figure 8. Examples of outputs of the Semblance and Radial Semblance modules for the analyses of LP and VLP events recorded on 23rd October 2010. Three sections of (a) Semblance and (b) Radial Semblance grids through the largest value node; the results shown are average distributions for 38 LPs (a) and 51 VLP (b), respectively; the grid of 5x5x2 km^3 (E-W, N-S and vertical directions) is interpolated to the Digital Elevation Model of Mt. Etna.

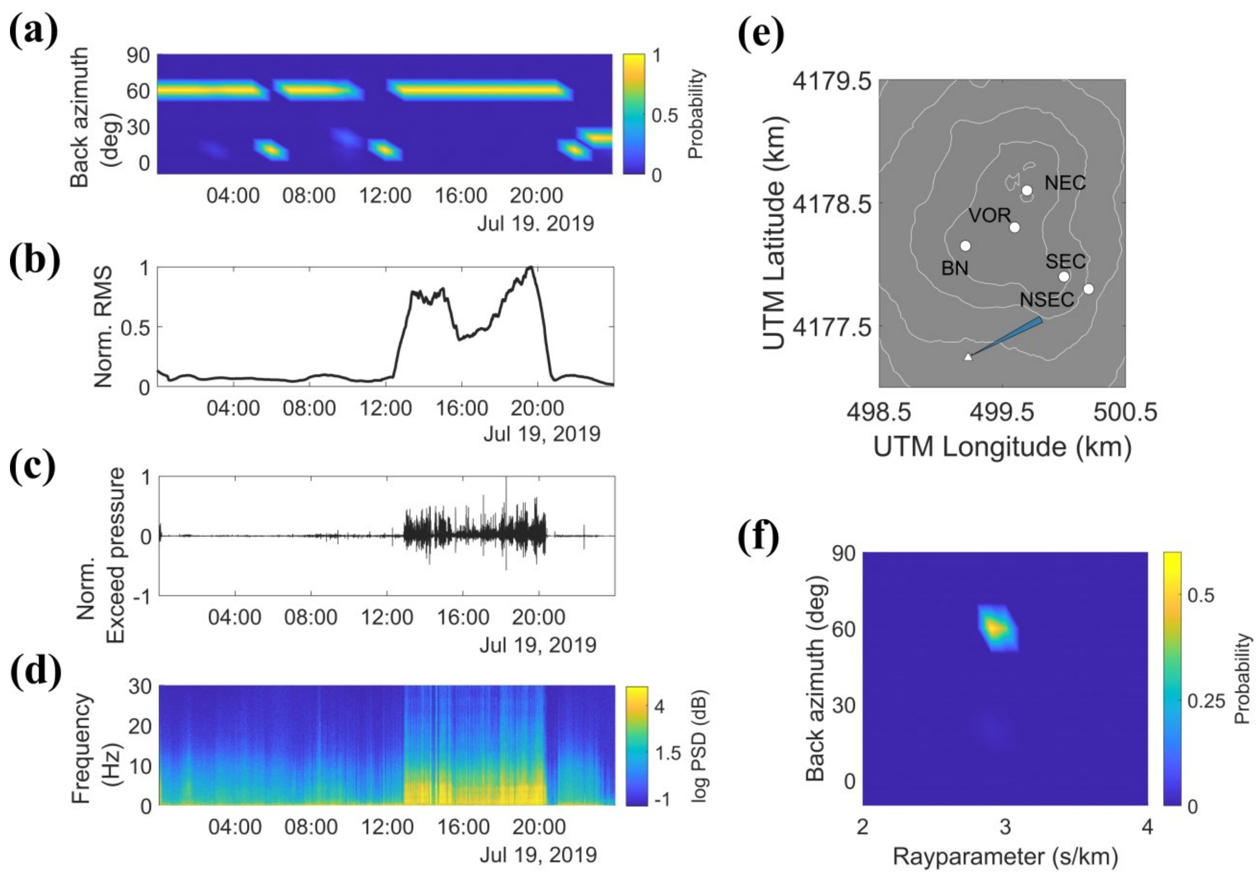

Figure 9. Output from the Signal viewer, Spectrogram and ZLC modules from analyses of infrasonic tremor recorded on 30th July 2011 at Mt. Etna, Italy. a) Temporal evolution of the array-calculated backazimuth, ranging between 50°N and 65°N. The ZLC analysis was performed on data were filtered in the 0.7-15 Hz frequency band. b) 1-hour long moving average of RMS

amplitudes in the 0.7-15 Hz frequency range at the central node of the array. c) Infrasound signal at the central node of the array. d) Spectrogram at the central node of the array. e) Polar histogram of backazimuth results in (a) and plotted on the Digital Elevation Model of the summit area of Mt. Etna with the main craters (white circles; Bocca Nuova: BN; Voragine: VOR; North-East Crater: NEC; South-East Crater: SEC; New South-East Crater: NSEC). f) Bi-variate distribution (2D histogram) of ray parameter and backazimuth, respectively.

APPENDICES

Table A1. Parameters for analysis of volcanic tremor recorded on 30th July 2011 using Beam Pattern, Spectrogram and ZLC modules.

Method	Settings	Waveform data	Output size	Timing
Beam Pattern	Frequency (Hz): 0.5-5.0 Frequency step (Hz): 0.5 Grid size (s^2/km^2): 2x2 Grid step (s/km): 0.05			Data processing (s): ~0.30
Spectrogram	Window (s): 60 N° samples spectra: 8192 High pass filter (Hz): 0.01 Averaging factor (min): 30	Sample rate (Hz): 100 Sample count: 8460000 N° sensors: 1 vertical component	~2.41 MB	Data processing (s): ~1.07 Data saving (s): ~0.52
RMS	Window (s): 10 Frequency band (Hz): 1.0-1.5 Averaging factor (min): 60	Sample rate (Hz): 100 Sample count: 8460000 N° sensors: 1 vertical component	~117 KB	Data processing (s): ~0.83 Data saving (s): ~0.15

ZLC	Window (s): 10 Frequency band (Hz): 1.0-1.5 Velocity waves (km/s): 1.6 km Max delay time (s): 4 Spline interpolation: True Histogram bin (min): 60 Correlation threshold: 0.75	Sample rate (Hz): 100 Sample count: 8460000 N° sensors: 5 vertical component	~579 KB	Data processing (s): ~23.83 Data processing with jackkinfe (s): ~88.09 Data saving (s): ~0.25

Table A2. Parameter for the analysis of LP and VLP events recorded on 23rd October 2010 using STA/LTA, SALPED, Semblance and Radial Semblance modules.

Method	Settings	Waveform data	Output size	Timing
STA/LTA	Frequency band (Hz): 0.01-0.15 STA window (s): 6 LTA window (s): 60 Detection threshold: 2.5 Window spectrogram (s): 5.28 Overlap window spectrogram (s): 5.20 N° samples spectra: 1024 Window polarization (s): 5	Sample rate (Hz): 100 Sample count: 8460000 N° sensors: 1 three components	~86.50 MB	Data processing (s): ~1.97 Spectral data processing (s): ~24.99 (~0.49 per event) Polarization data processing (s): ~19.38 (~0.38 per event) Data saving (s): ~51.29 (~1.01 per event)
SALPED	Central frequency brand (Hz): 0.5-1.2 Lower frequency band (Hz): 0.1-0.4 Upper frequency band (Hz): 3-10 Windows (s): ± 5 Detection threshold: 1.0 Window spectrogram (s): 1.28 Overlap window spectrogram (s): 1.20 N° samples spectra: 128 Window polarization (s): 2.5	Sample rate (Hz): 100 Sample count: 8460000 N° sensors: 1 three components	~11.70 MB	Data processing (s): ~2.24 Spectral data processing (s): ~17.10 (~0.45 per event) Polarization data processing (s): ~13.68 (~0.36 per event) Data saving (s): ~38.22 (~1.01 per event)

Semblance	Window (s): 2.5 Frequency band (Hz): 0.5-1.2 Central frequency (Hz): 1 Grid size (km^3): 5x5x2 Grid step (km): 0.1 Quality factor: 40 Velocity waves (km/s): 1.6 km Attenuation factor: 1	Sample rate (Hz): 100 Sample count: 1000 N° sensors: 7 three components N° events: 38	~12.10 MB	Data processing (s): ~28.72 (~0.75 per event) Data processing with jackkinfe (s): ~230 (~6.05 per event) Data saving (s): ~1.30
Radial Semblance	Window (s): 5 Frequency band (Hz): 0.01-0.15 Grid size (km^3): 5x5x2 Grid step (km): 0.1 Velocity waves (km/s): 1.6 km	Sample rate (Hz): 100 Sample count: 12000 N° sensors: 7 three components N° events: 51	~15. 30 MB	Data processing (s): ~211.76 (~4.15 per event) Data processing with jackkinfe (s): ~1 694.08 (~33.22 per event) Data saving (s): ~1.75

Table A3. Parameters for the analysis of infrasound recorded on 19th July 2019 using Spectrogram and ZLC modules.

Method	Settings	Waveform data	Output size	Timing
Spectrogram	Window (s): 60 N° samples spectra: 8192 High pass filter (Hz): 0.01 Averaging factor (min): 30	Sample rate (Hz): 100 Sample count: 8460000 N° sensors: 1 vertical component	~1.86 MB	Data processing (s): ~0.98 Data saving (s): ~0.37

RMS	Window (s): 10 Frequency band (Hz): 0.7-15 Averaging factor (min): 60	Sample rate (Hz): 100 Sample count: 8460000 N° sensors: 1 vertical component	~192 KB	Data processing (s): ~0.81 Data saving (s): ~0.35
ZLC	Window (s): 10 Frequency band (Hz): 0.7-15 Velocity waves (km/s): 0.354 km Max delay time (s): 4 Spline interpolation: True Histogram bin (min): 60 Correlation threshold: 0.75	Sample rate (Hz): 100 Sample count: 8460000 N° sensors: 6 vertical component	~460 KB	Data processing (s): ~24.01 Data processing with jackkinfe (s): ~87.54 Data saving (s): ~0.31

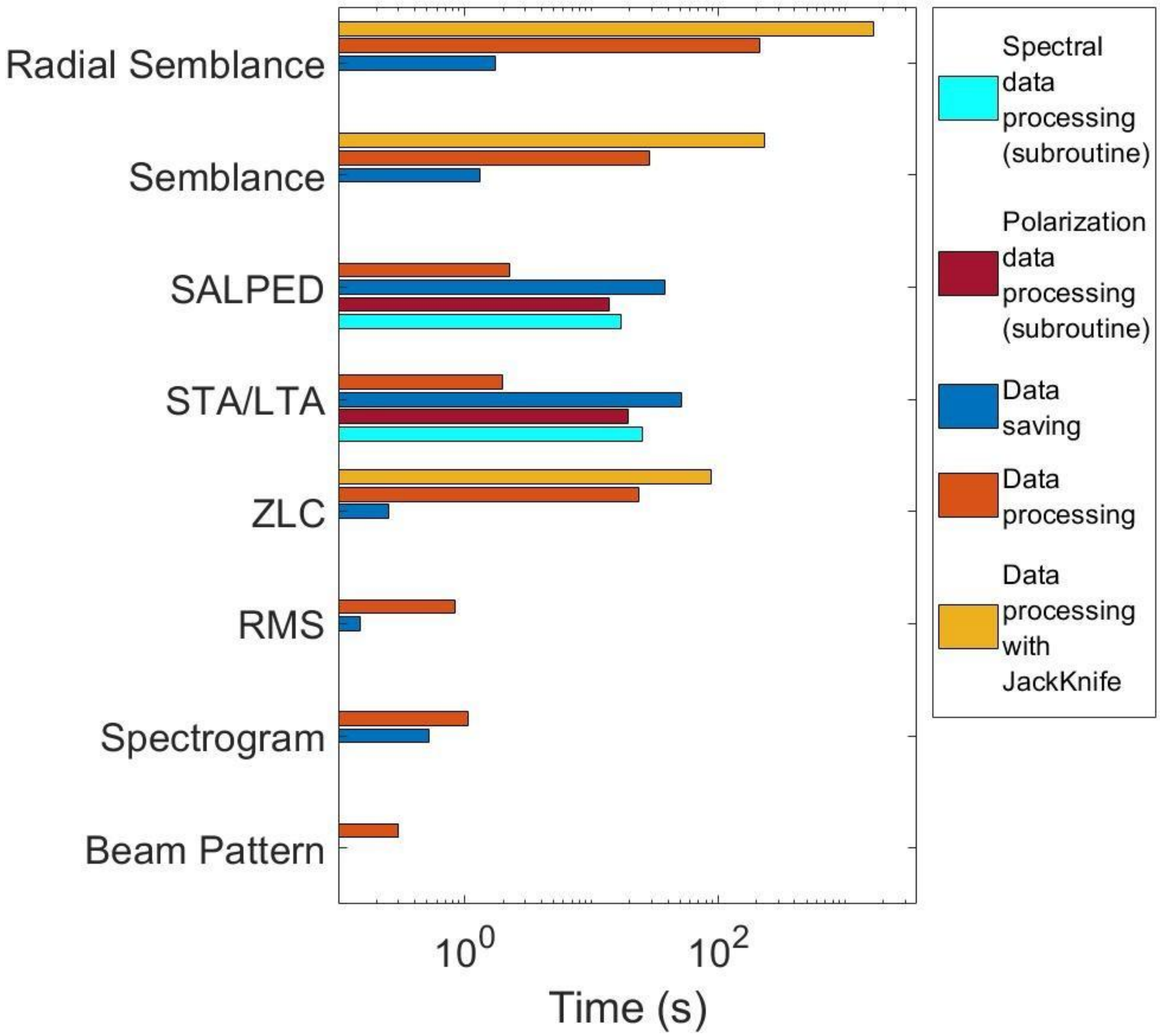

Figure A1. Software performance for Test Case study 1, 2 and 3. Each bar refers to the overall time required to perform the analyses summarised in the Tables A1, A2 and A3. The legend to the right-hand side of the diagram refers to the types of routines/subroutines activated during the processing of the data.